6C.6

CONDITIONS INFLUENCING HURRICANE EMILY'S (2005) PRECIPITATION PATTERNS, CONVECTION AND UPPER TROPOSPHERIC OUTFLOW

Kevin R. Quinlan, Daniel J. Cecil, and John Mecikalski
University of Alabama – Huntsville, Huntsville, AL

1. INTRODUCTION

Hurricane Emily (2005) became the earliest-forming category five hurricane on record in the Atlantic basin on 17 July 2005, becoming another standout storm in the record breaking hurricane season of 2005. The storm was monitored by the Tropical Cloud Systems and Processes (TCSP) field campaign that was conducted from July 1 – 27, 2005. Through the use of the ER-2 instruments, AMPR and EDOP, and GOES-11 infrared imagery, this study will analyze the eyewall structure during the morning hours of 17 July. Precipitation patterns will be determined using TRMM TMI, AMSR-E, and SSM/I and correlated with environment factors to determine the reasons behind the witnessed patterns. The upper-tropospheric outflow will be examined using GOES-11 satellite derived winds from CIMSS at the University of Wisconsin – Madison. A hypothesis will be examined linking the relationship between Inertial Available Kinetic Energy (IAKE) and convection in the inner radii of the storm. The primary purpose of this study is to better understand the relationship between tropical cyclone convection and the environmental effects impacting the system.

2. DATA AND METHODS

Data for the rainrate calculations were taken from the Remote Sensing Systems microwave-based product (Hilburn and Wentz 2007). These rainrates were then broken up by range and quadrant to create a time series of rainrates by quadrant for the life of the storm. This data was plotted alongside the U and V shear vectors for each point in the storm. The shear and rain rate data was then compared to determine if there were meaningful correlations between these two fields.

Rainrate data was also used to determine how well the convection near the center of the storm (radii $\leq$ 100 km) correlated with the IAKE field. IAKE fields were computed using the University of Wisconsin – Madison Non-hydrostatic model. This data was also broken up into quadrants in order to make all calculations comparable.

Data collected during ER-2 flight early on 17 July was analyzed to study the convection in the eyewall of a category 5 hurricane. The ER-2 made two transits across during the between 0750 UTC and 0850 UTC. The first transit encountered stronger than expected convection in the WNW eyewall. Convection was studied during the storm through the used of the Advanced Microwave Precipitation Radiometer (AMPR) and the ER-2 Doppler (EDOP) Radar. AMPR measurements were analyzed using the AMPR Precipitation Index (API) in the same manner as it was presented in Hood et al. (2006).

Radial mass flux plots were created through the use of the satellite derived wind algorithm developed at CIMSS and the University of Wisconsin – Madison. These plots were used to analyze the amount of mass flowing directly into or away from the center of the storm. These mass flux measurements were then compared with other upper-tropospheric measurements (NCEP Reanalysis and AOML dropsonde data) to determine what factors may have been affecting the environment around the storm.

Corresponding author address: Kevin R. Quinlan, UAH – NSSTC, 320 Sparkman Dr NW, Huntsville, AL 35805.
quinlan@nsstc.uah.edu

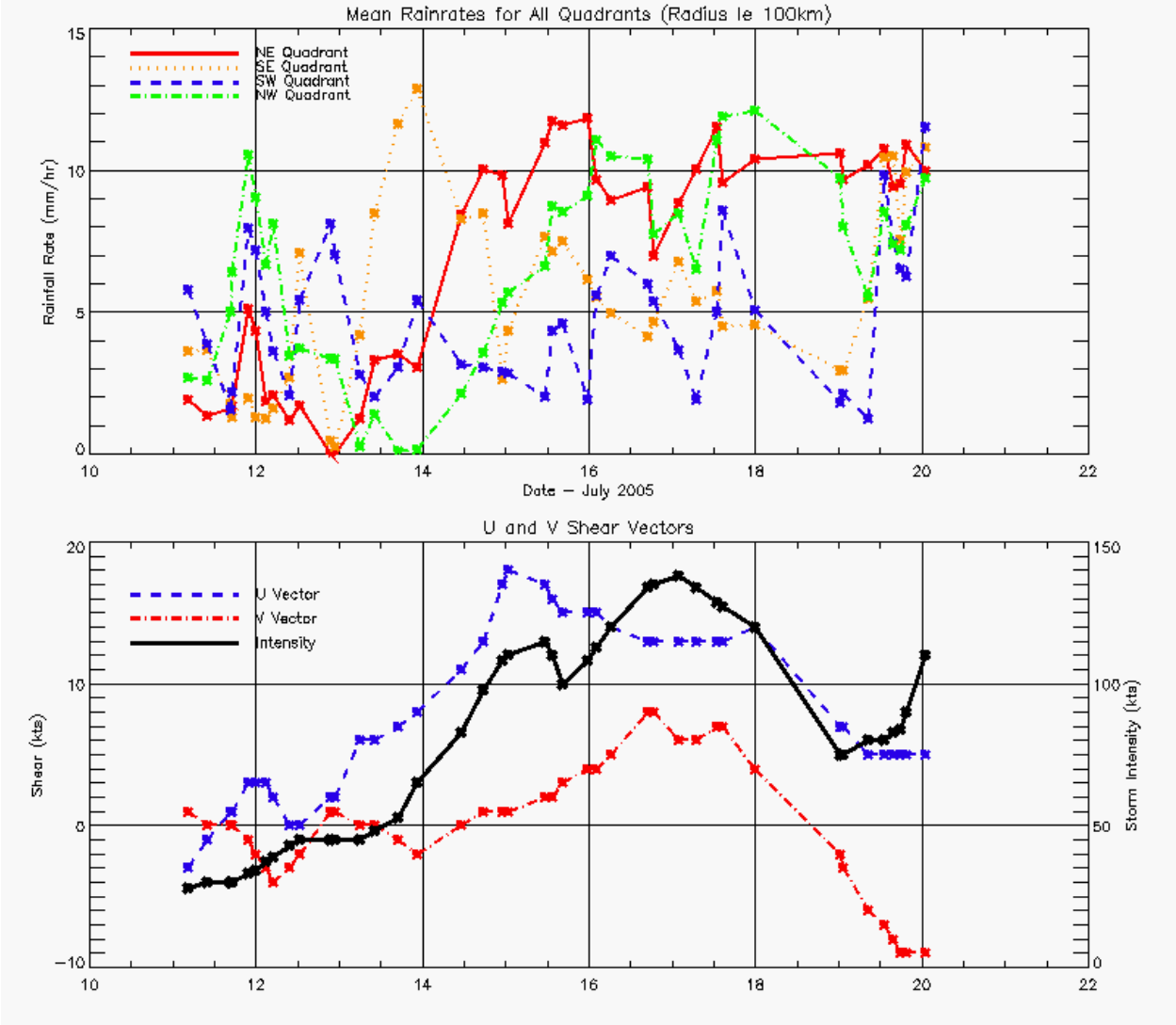

Figure 1. (top) Mean rainrates for each quadrant with a 0 - 100 km radius. (Bottom) U and V components of 200-850 hPa vertical shear vectors, and maximum sustained winds.

3. RESULTS

Figure 1 is a time series of the rainrates and the shear for Hurricane Emily. Beginning on July 11 and 12, the shear was weak with the westerly (U-component) increasing on July 13. During this time, the NW, SW, and NE quadrant rainrates decreased sharply on July 12, while the SE quadrant rain rates showed an increase. Following a brief period of decreasing rain rates, the SE quadrant increased substantially from about 0 mm/hr to about 13 mm/hr at about 00Z on July 14. This occurred during a time of increased westerly shear, which would put the SE quadrant in the downshear-right direction. This increase in precipitation goes against the current school of thought (Corbosiero and Molinari 2002; Cecil 2007), that convection should be increasing in the downshear-left direction. As the westerly shear continued to increase, and Emily continued to intensify on July 14 and 15, precipitation rates in the NE quadrant steadily increased as rates in the SE quadrant decreased. Rain rates also increased steadily in the NW quadrant during this time period. Rain rates become

concentrated in the NE and NW quadrants during the period of July 16 – 18, while the shear is predominantly from the west southwest. This is expected because these quadrants are in the downshear and downshear-left directions. This pattern continues until Emily moves over the Yucatan Peninsula on July 18; there are no rain rate observations during this time period as RSS retrievals are not made over land. Once Emily emerged into the Bay of Campeche, the shear weakened and became northwesterly. During this time period, the rain rates in the SW quadrant increased sharply on July 19, and the rain rates pattern overall became much more symmetric. This symmetry may be due in part to a change in the outflow patterns over the SW and SE quadrants.

The rainrates and the U-shear vector had a significant positive correlation in the northwest and northeast quadrants. These correlations were calculated for 6, 12 and 24 hour lead times as well as instantaneous times. Significant correlations with the U-component of the shear in the northern portions of the storm confirm that previous school of thought that precipitation will increase when down shear or down shear-left of the shear vector.

Figure 2 (top) shows the reflectivity from the EDOP radar as it passed over the southern portion of the eye. The figure shows a southeastern eyewall with the highest reflectivities at about 45 dBZ near the surface reaching to about 12 km. This is then followed by thin low-level clouds that are shown in the AMPR images (Fig. 3). After passing over the weakest reflectivities, the northwestern eyewall is defined by two areas of strong convection. The first area of convection was confined to about 7 km AGL and had reflectivities of close to 50 dBZ. The second area is the convective cell that caused the turbulence on the ER-2 flight.

The echo tops in this cell reached to just over 17 km (~56,000 ft) and it had a maximum reflectivity of over 60 dBZ at an altitude of 4 km (~13,400 ft) at 0752 UTC. EDOP observed reflectivities of 40 dBZ or greater up to an altitude of 14,550 m (~47,700 ft) and reflectivities of 50 dBZ or greater up to an altitude of about 8,325 m (~27,300 ft).

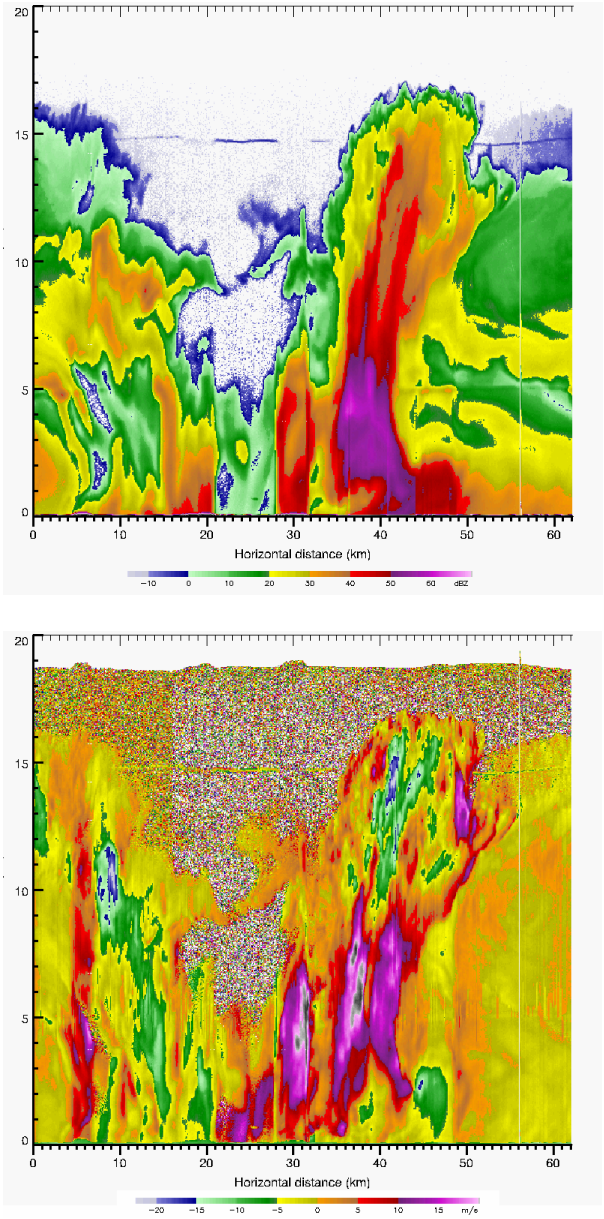

Figure 2. (top) EDOP Reflectivity in a east southeast - west northwest direction across eye of Hurricane Emily from 0750 UTC - 0755 UTC on 17 July. (bottom) EDOP vertical velocity during same timeframe. A fallspeed correction has been applied. It is also possible that horizontal wind has been aliased in where the radar beam is not pointed directly down.

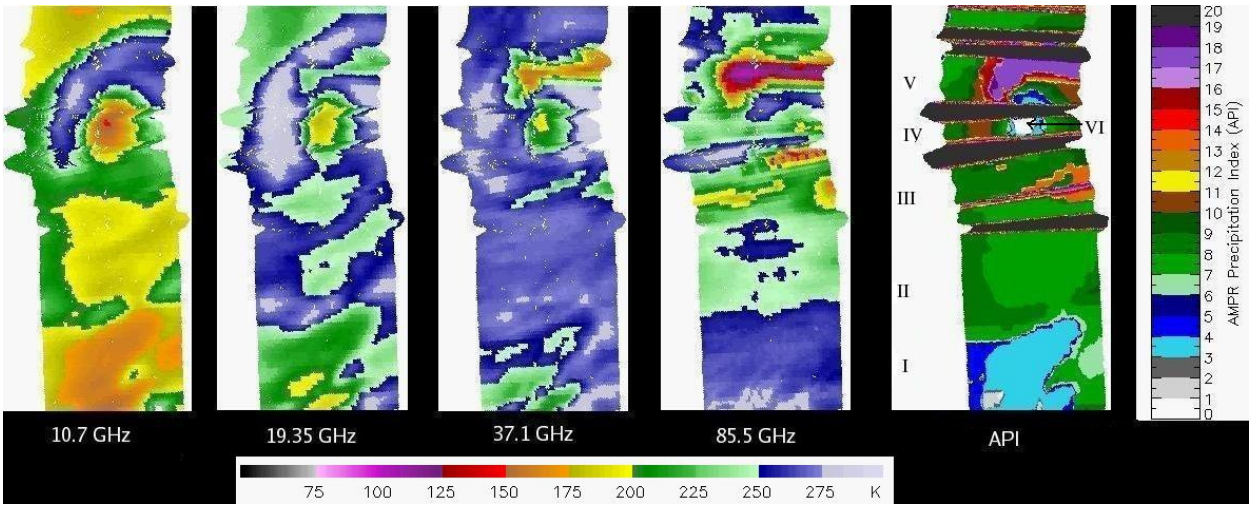

Figure 3. Horizontal mapping of the four AMPR channels and API. Time of ER-2 flight for this image was 0746 UTC (ESE – bottom) - 0755 UTC (WNW – top) on July 17. API color scale is shown along the right side of the figure. The AMPR color scale is shown along the bottom of the image.

Figure 2 shows the same outward sloping eyewall as suggested in the AMPR data. After this cell, reflectivities greatly diminished as the ER-2 began to pass over areas of stratiform rain. While over this portion of the storm, the brightband becomes visible at about 5,000 m (16,400 ft).

AMPR data was used to study the precipitation patterns in and around the eyewall during the ER-2 transit. Fig. 3 depicts the first eye crossing, showing the four AMPR channels and the API described in Hood et al. (2006). Each panel has been rotated to maximize space and for ease of viewing. The bottom of each panel is the east southeast side of the eyewall, and the top of each panel is the WNW side of the eyewall.

The image is broken up into segments, labeled I - VI based on the patterns in the data. The first area, segment I, of the swath to be examined is the area at the bottom of the image that falls into the API 3 (light blue), Ice Level 0 (IL0) category. According to the criteria set forth by Hood et al. (2006), this area is determined to have no precipitation-sized ice in the clouds and have light-moderate rain. This is most likely an area of stratiform rain. The high Tb85 values suggest that this area has little or no ice scattering occurring. This area corresponds to the orange area in the Tb10 panel that has TB temperatures between 160 – 175 K. The green areas, labeled segment II, fall into API values of 7 and 8, and IL1. In these areas, it has been determined that a moderate amount of precipitation ice exists in the cloud because Tb85 < Tb37. The pixels that fall into an API value of 7 and Tb10 values of 175K to 200 K match up when comparing the two panels. A Tb10 value of 200 – 225 K is portrayed for pixels with API values of 8, suggesting greater liquid rain rates.

Segment III, the first example of ice level 2 values are found along the right side of the swath. This region is expected to have greater precipitation ice due to its close proximity to the southeastern eyewall. This area is comprised mostly of API values of 13, which indicate heavy ice and a rain level value of 3. The ice in the clouds for this region is large enough to scatter radiation in the 37 GHz channel and has Tb10 levels between 200K and 225 K. The next area of interest, IV, is the area left of the eye in the

next swath. This area is comprised mostly of API values of 10, which is the highest API value in IL1. This area showed that the ice was large enough to scatter radiation from only the 85 GHz channel and had Tb10 values greater than 250 K. These pixels correspond very well with the dark blue (approximately 250 K) pixels that are seen in the 10.7 GHz channel to the left of the eyewall, suggesting heavier rain.

The highest API values for this eyewall pass were found in segment V, as indicated by the purple colors representing API values of 17. These pixels fall into the IL3 category because the ice is large enough to scatter radiation in the 19.35 GHz channel. These pixels also have Tb10 values between 250K and 275K. This area naturally follows the lower TB seen in the successive panels for 19.35, 37.1, and 85.5 GHz.

The last region to be examined for this ER-2 pass is the eye itself, which is labeled segment VI. The center of the eye returned an API value of 0, which indicated that there were clear conditions. This, however, is not seen in the EDOP data, which shows shallow clouds between 2 and 3 km from the surface. It should be noted that the API is not intended to identify regions that are truly cloud-free. Tb10 values less than 160 K and Tb37 values greater than 215 are seen in the "clear" area. API values increase sequentially from 0 in the eye to 17 in the eyewall. This pattern is suggestive of the outward-sloping eyewall's stadium effect. Moving outward from the eye, we first encounter heavy liquid rain and then progressively thicker precipitation layers.

The EDOP and AMPR both highlight the WNW eyewall as having intense convection during this 0750-0755 UTC transit. High reflectivities (> 40 dBZ) reach near the tropopause. Updrafts exceeding 30 m/s are indicated, although there is some uncertainty in the data quality. Substantial scattering by large ice particles is seen in AMPR's 85, 37, and 19 GHz channels, with a trace even suggested in the 10 GHz channel. A sequence of infrared imagery (not shown) indicates that the ER-2 arrived at the same time as a convective burst developing along the WNW eyewall at 0753 UTC. The cold cloud tops associated with this cell were first seen in the infrared imagery at 0750 UTC. By 0755, the cold cloud tops were already advected into the southwest quadrant of the storm.

REFERENCES

Cecil, D. J. (2007), Satellite-derived rain rates in vertically sheared tropical cyclones, Geophys. Res. Lett., 34, L02811, doi:10.1029/2006GL027942.

Corbosiero, K.L., and J. Molinari, 2002: The Effects of Vertical Wind Shear on the Distribution of Convection in Tropical Cyclones. *Mon. Wea. Rev.*, **130**, 2110–2123.

Hilburn, K.A., and F.J. Wentz, 2008: Intercalibrated Passive Microwave Rain Products from the Unified Microwave Ocean Retrieval Algorithm (UMORA). *J. Appl. Meteor. Climatol.*, **47**, 778-794

Hood, R.E., D.J. Cecil, F.J. LaFontaine, R.J. Blakeslee, D.M. Mach, G.M. Heymsfield, F.D. Marks, E.J. Zipser, and M. Goodman, 2006: Classification of Tropical Oceanic Precipitation using High-Altitude Aircraft Microwave and Electric Field Measurements. *J. Atmos. Sci.*, **63**, 218–233.

Mecikalski, J.R., and G.J. Tripoli, 1998: Inertial Available Kinetic Energy and the Dynamics of Tropical Plume Formation. *Mon. Wea. Rev.*, **126**, 2200–2216.

Acknowledgments:
This work was supported by NASA through the Tropical Cloud Systems and Processes (TCSP) program.

I would like to thank Chris Velden and CIMSS for their help in providing data and support. I would also like to thank Remote Sensing Systems for providing the rain rate estimates and Matt Wingo for his help with the rain rates and vertical wind shear.